Origin of the strong optical nonlinearity of tellurium oxide–based compounds: The specific case of BaTe2O6

David Hamani, Antoine Plat, Maggy Colas, Julie Cornette, Olivier Masson, Philippe Thomas

Origin of the strong optical nonlinearity of tellurium oxide–based compounds: the specific case of $BaTe_2O_6$

D. Hamani *, A. Plat, M. Colas, J. Cornette, O. Masson, A. P. Mirgorodsky, P. Thomas

Laboratoire Science des Procédés Céramiques et de Traitements de Surface (SPCTS) – UMR CNRS 7315, Université de Limoges, Centre Européen de la Céramique, 12 rue Atlantis, 87068 Limoges Cedex, France.

* Corresponding author: David Hamani, E-mail: david.hamani@unilim.fr

Keywords

tellurium (IV) oxide; tellurium (VI) oxide; optical nonlinearity; lattice dynamics; *ab initio*

Highlights

- Vibrational analysis of the $BaTe_2O_6$ phase reported for the first time.
- Exceptional TeO^{2+} fragment situated in the $Te^{IV}O_5$ coordination sphere.
- Relevant relationships between the long Te^{IV}-O bonds and the $\chi^{(3)}$ susceptibility.

Abstract

This paper is a contribution to the understanding of the crystal chemistry origin of the strong nonlinear optical properties of tellurium oxide–based compounds. The particular case of the $BaTe_2O_6$ ($BaTe^{IV}Te^{VI}O_6$) phase has been investigated. The structure refinement using single crystal X-ray diffraction confirms that the Te^{IV} atom is located in an unclassical TeO_5 environment with one exceptionally short Te-O bond (1.82 Å) and four long ones (2.12 Å). The vibrational analysis points out that in this environment, from the spectrochemical point of view, the short bond is at the origin of a quasi-isolated $Te^{IV}O^{2+}$ molecular ion whereas the

four longer bonds traduce weak interactions. Relationships have been established between the Te^{IV}-O bond lengths and the $\chi^{(3)}$ susceptibility. The four long bonds, belonging practically to the xz–plane and involving the Te^{IV} d-orbitals contribution, are at the origin of the high $\chi^{(3)}_{xxxx}$ and $\chi^{(3)}_{zzzz}$ values (30.0 and 44.3 × 10^{-13} esu respectively). The short Te-O bond, directed along the y–direction, is responsible for the lower $\chi^{(3)}_{yyyy}$ value (3.2 × 10^{-13} esu). This study is the first obvious confirmation for a real crystal lattice of the high superiority of the nonlinear polarizability of the weak intermolecular Te-O bonds over that of the strong molecular Te-O ones.

1. Introduction

The 'structure-properties' problem aims at understanding the relationships between fundamental physical characteristics of crystal lattices and the nature of their interatomic bonding. It always remains an intriguing point for the crystal chemistry and fundamental material science. The present paper focuses on the peculiarities of the atomic arrangement and the extraordinarily high nonlinear optical characteristics of tellurium oxide-based materials, more specifically in the $BaTe_2O_6$ ($BaTe^{IV}Te^{VI}O_6$) crystal lattice. From the point of view of solid state chemistry, the peculiarity of $BaTe_2O_6$ is the electronic structure of the coordination spheres of the Te^{IV} atoms, which can be at the origin of extraordinary polarization properties.

Historically, it was revealed about twenty years ago that the $\chi^{(3)}$ susceptibility for pure TeO_2 glass is about fifty times as high as that for SiO_2 [1] (and was recently confirmed for their crystalline forms as well [2,3]). This fact has aroused considerable interest in the relevant studies which initially were only slightly or not at all concerned with the question: where does this high nonlinear susceptibility come from? It was generally accepted that the Te^{IV} lone electron pairs (always present in those compounds) account for such a property [4]. However, the results of subsequent quantum chemistry *ab initio* considerations of different TeO_2 cluster models have shown that it is not the case [5–7], and the origin of those properties should be attributed to specific Te-O linkages occurring in the TeO_4 polyhedra which build up the molecular polymers or the crystal lattices of TeO_2. In every polyhedron, there are two weak linkages having length of about 2.1 Å, while the rest two (about 1.9 Å in length) form a TeO_2 molecular–like unit whose geometry is close to that of the isolated molecule. So, the last mentioned fact allows regarding the TeO_2 lattices (three polymorphs α– [8], β– [9] and γ–TeO_2 [10]) as molecular crystals in which the long linkages are intermolecular bonds. According to the *ab initio* calculation results, in which the total nonlinear polarizability values

of TeO_2–made clusters were separated into intramolecular and intermolecular contributions, the weak intermolecular Te-O bonds represent the main source of the extraordinarily high $\chi^{(3)}$ susceptibility for solid forms of TeO_2.

Generally, TeO_2–based complex oxides are constituted of TeO_4 and/or TeO_{3+1} and/or TeO_3 polyhedra which depend on the nature and quantity of the added modifier oxide (see Figure 1 and for example [11–15]). Very little information on the presence of Te^{IV} coordination spheres other than the above-mentioned can be found in the literature. One example was evidenced in the $Cs_2Te_4O_{12}$ ($Cs_2Te^{IV}Te^{VI}{}_3O_{12}$) crystal lattice [16] in which the Te^{IV} atom is centred in a regular $Te^{IV}O_6$ octahedron formed by six Te-O bonds (2.10 Å, see Figure 1). The vibrational spectroscopy study complemented by the lattice dynamics analysis [17] allowed to conclude that the Te^{4+} ion has no localized lone pair and, jointly with the Cs^+ ions, play the role of quasi-isolated cations, implying that this compound is a tellurate (but not tellurite) with a complex $[Te^{VI}{}_3O_{12}]^{6-}$ anion. Another unusual type of polyhedron is found in the $BaTe_2O_6$ ($BaTe^{IV}Te^{VI}O_6$) crystal lattice [18]: it contains a particular $Te^{IV}O_5$ symmetric tetragonal pyramid in which the Te^{IV} atom forms one exceptionally short Te-O bond (1.83 Å) in the opposite direction of the Te^{IV} lone electron pair, and four much longer equivalent Te-O bonds (2.13 Å) (Figure 1). The longest Te-O separations can be readily specified by a mainly electrostatic attraction, the shortest bond has an essentially covalent nature and therefore can be considered as a quasi-isolated molecular-like TeO^{2+} entity, which provokes a special interest to the $BaTe_2O_6$ crystal chemistry study.

It will be shown in this paper that the peculiarities of the $BaTe_2O_6$ structure offers a possibility to clarify in direct manner the contribution of the different Te-O bond types on the nonlinear optical properties. Therefore, as a starting step of this work, the crystal structure of the $BaTe_2O_6$ compound was reinvestigated by single crystal X-ray diffraction. This study was coupled with the analysis of the vibrational spectra (Raman and infrared spectra are presented

for the first time) obtained from the experiment and interpreted by using the relevant first-principles and empirical calculations.

The results obtained for the $BaTe_2O_6$ compound were interpreted from the crystal chemistry point of view in focusing our attention on the TeO^{2+} fragment situated in the TeO_5 coordination sphere around Te^{IV} atoms. These data were used to discuss the central subjects of this study: the relationships between the structural peculiarities of this coordination sphere in the $BaTe_2O_6$ phase and the linear and nonlinear optical characteristics, namely the tensors of linear and second-order nonlinear susceptibilities ($\chi^{(1)}$ and $\chi^{(3)}$, respectively) which were obtained by means of quantum chemistry *ab initio* calculations. Indeed, the calculations counterbalance the lack of experimental measurements due to the difficulty of growing large single crystals suitable for optical measurements.

The present paper is organized in the following manner. The experimental and calculation methods are exposed in part 2. The results are presented and discussed in parts 3 and 4 respectively, and concluding remarks are given in part 5.

2. Experimental and calculation methods

2.1. Synthesis

First, the basic material, TeO_2, was prepared by decomposing a commercial ortho-telluric acid H_6TeO_6 (Aldrich, 99.9%) at 550 °C for 24 h. A mixture was then obtained by adding stoichiometric amounts of commercial $BaCO_3$ (Aldrich, 99+%) to TeO_2. Single crystals of $BaTe_2O_6$ phase were synthesized, by melting the mixture under air atmosphere at 710 °C for 10 h in a gold crucible. The melt was first slowly cooled down at 1 °C.h^{-1} to 645 °C and then at 10 °C.h^{-1} to room temperature. A single crystal suitable for structural determination using X-ray diffraction was selected using a polarized light optical microscope.

2.2. Structural characterization

Intensity data were collected using a Bruker-Nonius KappaCCD area-detector diffractometer (Mo K_α radiation). The crystal data, data collection, refinement conditions and computing details are pointed out in Table 1.

The phase was analysed by Raman and infrared spectroscopy as well. The Raman spectrum was recorded at ambient conditions in the 30-900 cm^{-1} range using a spectrometer (Jobin-Yvon Horiba T64000) equipped with an Ar^+ laser (514.5 nm exciting line) and a CCD detector in a backscattering geometry. A good signal/noise ratio required two scans of 20 seconds each. The focalization was done through a microscope (x50 LWD) and the diameter of the laser spot focused on the sample was about 1 µm. Measurements were performed at a power of 200 mW of the exciting line. The spectral resolution was about 2.5 cm^{-1} at the exciting line (1800 grooves.mm^{-1} grating). The infrared spectrum was recorded in the absorbance mode on a Fourier transform spectrophotometer (Thermo Fisher Nicolet 6700) using the polyethylene and CsI pressed technique in the 80-500 and 500-900 cm^{-1} ranges, respectively.

The modelling consists in calculating the vibrational spectra of the structure (*i.e.* the wavenumbers and the types of vibrations) in order to assign the experimental bands. First-principles calculations were carried out using the CRYSTAL06 software [19,20] to obtain self-consistent information about the structure, wavenumbers, symmetry, eigenvectors and infrared intensities (but not Raman intensities) of the zone centre vibrations of $BaTe_2O_6$, as well as about the Te-O interatomic overlap population in various TeO_2– and TeO_3–based compounds using the same *ab initio* routine. The computational technique was based on the density functional theory (DFT) using the Becke's three-parameter hybrid nonlocal exchange functional [21] combined with the Lee-Yang-Parr gradient-corrected correlation functional B3LYP [22]. The number of k-points used to describe the irreducible part of the Brillouin

zone was chosen to be 27. The LADY program [23] was used to perform an empirical lattice dynamical model treatment of the $BaTe_2O_6$ structure in order to interpret its vibrational spectrum. This program provides the information about the wavenumbers and eigenvectors of normal modes of crystal vibrations. The experimental crystallographic data (space group, lattice parameters, and atomic coordinates) were used jointly with the data on the force constants of the relevant interatomic bonds using the Valence Force Field (VFF) model. These data are in the form of an empirical curve displaying the dependence of the bond force constant values on the interatomic distance [24].

2.3. Optical properties

Ab initio method was used in order to tackle the problem that unfortunately no experimental measurement was adapted due to the insufficient size (the tenth of millimetre) of the synthesized single crystals. Density functional first-principles simulations based on a numerical atomic orbital method [3,25] were thus executed to calculate the tensor elements of the linear $\chi^{(1)}$ susceptibility and of the second-order nonlinear $\chi^{(3)}$ susceptibility. Calculations were carried out using the SIESTA code [26] within the generalized gradient approximation (GGA) and the Perdew-Burke-Ernzerhof (PBE) functional [27,28] to simulate the electronic exchange and correlation. Core electrons were replaced by *ab initio* norm-conserving pseudopotentials generated with the Troullier-Martins scheme [29] in the Kleinman-Bylander fully nonlocal separable representation [30].

3. Results

The $BaTe_2O_6$ phase crystallizes in the orthorhombic space group n°63 (Cmcm, D_{2h}^{17} point group) with the unit cell parameters: a = 5.562(2) Å, b = 12.773(5) Å, c = 7.318(3) Å, V = 519.9(3) $Å^3$ and Z = 4 (*cf.* Figure 2 (a)). In addition to Table 1, structural characteristics

(atomic coordinates, displacement parameters and interatomic distances) obtained from single crystal X-ray diffraction are presented in Table 2. These results are in agreement with those of Koçak *et al.* [18]. The calculation of the bond valence sums from the interatomic distances, using the Adams' constants [31,32], emphasizes the existence of barium II (1.8 valence unit), tellurium IV (4.2 v.u.) and tellurium VI (6.1 v.u.).

The experimental Raman and infrared spectra are given in Figure 3 and completed with *ab initio* calculations. The Raman spectrum obtained by the empirical lattice dynamical model is shown in Figure 4 for two cases: a 'full-lattice' treatment (Figure 4 (a)) and another without taking into account the contribution of the long Te^{IV}-$O_{(3)}$ contacts (2.12 Å) (Figure 4 (b)). The relevant wavenumber positions are reported in Table 3 in which the overall calculated values are close to the experimental ones. The primitive cell of the $BaTe_2O_6$ lattice contains 18 atoms (two formula units). Correspondingly, 51 optical vibrational modes related to the Γ-point of the Brillouin zone are distributed among the irreducible representations of the D_{2h}[17] point group as follows: $\Gamma = 7A_g + 4A_u + 7B_{1g} + 8B_{1u} + 3B_{2g} + 8B_{2u} + 7B_{3g} + 7B_{3u}$. 24 g-modes are Raman-active ($7A_g + 7B_{1g} + 3B_{2g} + 7B_{3g}$) and 23 u-modes are IR-active ($8B_{1u(z)} + 8B_{2u(y)} + 7B_{3u(x)}$) (the $4A_u$ modes are IR-inactive). Since the Te^{VI} atoms occupy inversion centres, their displacements are absent in the g-modes.

The Figure 5 presents the Te-O interatomic overlap population versus the experimental length obtained by *ab initio* calculations for several TeO_2– and TeO_3–based compounds (taken from [17]) and is completed with the calculated data for the $BaTe_2O_6$ compound. The results for the $\chi^{(1)}$ and $\chi^{(3)}$ susceptibilities obtained by *ab initio* calculations are given in Table 4. For the $\chi^{(1)}$ tensor, the xx–, yy– and zz– elements have close values (respectively 4.2, 2.3 and 3.4), traducing an isotropy of this physical quantity. The remarkable point is revealed for the $\chi^{(3)}$ tensor: the values of the xxxx– and zzzz–elements (30.0×10^{-13} esu and 44.3×10^{-13} esu) are of the same order of magnitude than those for α-TeO_2 [3] and are about ten times higher than

that of the yyyy–element (3.2×10^{-13} esu). The former characterize the induced polarization along the x– and z–direction respectively while the latter characterizes it along the y–direction.

4. Discussion

4.1. Structural analysis from X-ray diffraction data

The mixed $BaTe_2O_6$ structure can be described at first sight as a layered structure. Every layer is made of infinite linear chains of $Te^{VI}O_6$ octahedra linked by vertices, two chains being linked by $Te^{IV}O_5$ tetragonal pyramids. Every $Te^{VI}O_6$ octahedron presents two Te^{VI}-$O_{(1)}$ bridging bonds with two other octahedra and four Te^{VI}-$O_{(3)}$ bridging bonds with four $Te^{IV}O_5$ polyhedra. The barium atoms lie between the layers. The Te^{IV} atom presents a pentacoordinated environment of O atoms with a short Te^{IV}-$O_{(2)}$ bond (1.82 Å) and four equivalent long Te^{IV}-$O_{(3)}$ bonds (2.12 Å), the Te^{IV} lone electron pair being opposed to the direction of the short bond. The Te^{VI} atom is placed at the centre of a slightly deformed octahedron of O atoms with four equivalent Te^{VI}-$O_{(3)}$ bonds (1.91 Å) and two equivalent Te^{VI}-$O_{(1)}$ bonds (1.92 Å) (Figure 2 (b)). Thus the structure presents symmetric Te^{VI}-$O_{(1)}$-Te^{VI} bridges (with a bridge angle of 143.7°) and asymmetric Te^{IV}-$O_{(3)}$-Te^{VI} bridges (with a bridge angle of 121.0°). The Ba atom is at the centre of a deformed 10-coordinated polyhedron of O atoms with two equivalent Ba-$O_{(2)}$ distances (2.86 Å), four equivalent Ba-$O_{(3)}$ distances (2.98 Å) and four other equivalent Ba-$O_{(3)}$ distances (3.01 Å) (Figure 2 (c)).

4.2. Structural analysis from vibrational spectra

In the above-presented structural description, by using pure geometrical criteria, all the O atoms are mentioned as bridging ones. Now, to perform a qualitative analysis of the vibrational modes related to the Te-O bonds, we address ourselves mainly to their chemical

nature. Let us look at the experimental Raman spectrum presented in Figures 3 and 4. It is dominated by two A_g bands above 600 cm^{-1} related to the stretching modes of the Te^{IV}-$O_{(2)}$ and Te^{VI}-$O_{(3)}$ terminal bonds and one A_g band near 515 cm^{-1} related to the bending mode of the Te^{VI}-$O_{(1)}$-Te^{VI} bridges. Such spectrum is inherent to a lattice containing chain like fragments [33].

To verify the objectivity of such attributions, and to make our analysis more definitive and more quantitative, we turn our attention to the results of the empirical model lattice dynamical treatment. Taking into account the argumentation relating to the nature of the axial bonds (having the length of 2.12 Å) in the TeO_4 polyhedra in the paratellurite α-TeO_2 lattice [24], we state our belief that the interatomic Te-O separations longer than 2.1 Å should be omitted from our analysis as being electrostatic contacts rather than covalent bonds. Two kinds of treatments were carried out to model the Raman spectrum: a 'full-lattice' treatment considering all the interatomic force constants including the Te^{IV}-$O_{(3)}$ contacts of length of 2.12 Å (Figure 4 (a)) and a second one without using the Te^{IV}-$O_{(3)}$ force constants *i.e.* these contacts are considered as weak interactions and are in that case simply ignored (Figure 4 (b)). The relevant data are given in Table 3. Firstly, the 'full-lattice' modelled spectrum is in accordance with the experimental spectrum, the main bands above 400 cm^{-1} being well reproduced. Secondly, the two modelled spectra are very similar: without considering the Te^{IV}-$O_{(3)}$ contacts, wavenumbers are only slightly shifted towards the low wavenumbers. Thus, the modelling consequently emphasizes the presence of quasi-isolated $[Te^{IV}O]^{2+}$ molecular ions.

Consequently, the more adequate form of the crystal formula should be Ba ($Te^{IV}O$) $Te^{VI}O_5$, defining an oxytellurate of Ba^{2+} and Te^{4+}. It implies that the anionic part is comprised of $[Te^{VI}O_5]^{4-}$ infinite chain-like tellurate anions built up from $Te^{VI}O_6$ octahedra. The cationic part consists of isolated Ba^{2+} ions and $[Te^{IV}O]^{2+}$ molecular ions. Terminal Te^{VI}-$O_{(3)}$ bonds

(1.91 Å), Te^{VI}-$O_{(1)}$-Te^{VI} bridges (1.92 Å) and Te^{IV}-$O_{(2)}$ bonds (1.82 Å) are thus found in the lattice.

Our revision of the $BaTe_2O_6$ crystalline structure indicates that the interatomic distance within the TeO^{2+} entity (1.82 Å) is, to the best of our knowledge, the smallest of all those occurring for Te-O bonding. It represents a unique molecular-like entity in which the interatomic bonding is the strongest among Te-O contacts. To clarify its chemical nature, the $Te^{IV}O_5$ polyhedron must be considered with more details. One contact corresponds to the TeO^{2+} 'molecule' and the rest four, representing the longest and weakest Te-O chemical linkages in the $BaTe_2O_6$ lattice, are intermolecular bonds whose length (2.12 Å) is equal to that in the α-TeO_2 lattice which is the fundamental structure of crystalline TeO_2 having quasi-molecular constitution. Let us recall that the extraordinarily high $\chi^{(3)}$ susceptibility of TeO_2–based materials is attributed to those intermolecular bonds [5–7]. In this connection, it is interesting to look at the key features of valence electronic cloud distributions in the two just mentioned lattices within the framework of the 'molecule in lattice' approach.

4.3. Chemical aspect of the Te-O bonding: bond orders in α-TeO_2 and $BaTe_2O_6$

Let us approximately estimate the bond orders using the overlap populations noticed in Figure 5. For the $Te^{IV}O_4$ polyhedron in α-TeO_2, the overlap population is equal to 0.141 for each of the two short equatorial bonds (1.88 Å) and 0.043 for each of the two long axial bonds (2.12 Å) so a total overlap population of 0.368. In an isolated TeO_2 molecule, the order of each Te-O bond (1.83 Å [34]) is equal to 2 and it can be thought that the initial cloud of 8 (4x2) electrons forming the two bonds of the isolated molecule is divided in the α-TeO_2 lattice between the intramolecular and the intermolecular clouds in the same proportion than that of the overlap populations. Thus the intramolecular clouds would contain 6 (3x2) electrons (so a bond order of 1.5), and 2 (1x2) electrons would belong to the intermolecular clouds (so a bond order of 0.5), this result being consistent with those of Yakovlev *et al.* [35].

Reasoning in the same manner for the $Te^{IV}O_5$ polyhedron in $BaTe_2O_6$, we notice an overlap population of 0.229 for the short Te-$O_{(2)}$ bond and 0.042 for each of the four long Te-$O_{(3)}$ bonds so a total overlap population of 0.397. In the virtual isolated TeO^{2+} molecule, the bond order is equal to 3 and we can think that the cloud of 6 bonding electrons would be distributed in the TeO_5 polyhedron of the $BaTe_2O_6$ lattice in such a way that 3.5 electrons should be attributed to the intramolecular bond (so a bond order of 1.8) and 2.5 electrons (0.625x4) would be given to the intermolecular bonds (so a bond order of 0.3).

Thus, in α-TeO_2 and $BaTe_2O_6$, the intermolecular Te-O bonds seem to keep their individual electronic features. Consequently, one may expect that these bonds should be the main source of the $\chi^{(3)}$ susceptibility of $BaTe_2O_6$. It is important to underline that, in contrast to the α-TeO_2 lattice in which the Te-O bonds are always oriented in general directions, in the $BaTe_2O_6$ lattice, all the TeO^{2+} ions lie strictly along the y axis, and the longest Te-$O_{(3)}$ linkages lie practically in the xz–plane. Keeping in mind this fact, we direct our attention to the results of the $\chi^{(1)}$ and $\chi^{(3)}$ susceptibilities of the $BaTe_2O_6$ compound.

4.4. Optical properties particularities

The corner stone of the next consideration is the conception of localized dipoles associated with the chemical bonds, which should allow us to connect the $\chi^{(1)}$– and $\chi^{(3)}$–tensor particularities directly with the $BaTe_2O_6$ geometry features. The most noticeable particularity of the $\chi^{(3)}$–tensor is that its xxxx– and zzzz–elements are more than ten times as large as the yyyy–elements (Table 4). The $Te^{VI}O_6$ octahedra and the Ba^{2+} ions are quasi-isotropic and thus cannot be responsible for a huge difference of those elements, which however is apparently attributable to the sharp anisotropy of the electron cloud distribution inside the $Te^{IV}O_5$ tetragonal pyramid. This clarifies why the nonlinearity of a polarization effect in the xz–plane is so much larger than that in the y–direction: the dipole moments of the four weak bonds lie practically in that plane, thus playing a primary role in the effect under consideration. As to

the role of the TeO^{2+} entity, its contribution is localized in the y–direction polarization, whose nonlinearity is quite humble. These results are the first obvious confirmation of the strong superiority of the nonlinear polarizability of the weak intermolecular Te-O contacts over that of the strong molecular Te-O bonds, which is revealed here not for virtual molecular clusters [5–7] but for a real crystal lattice. As an intriguing point, we wish to note that in contrast to the $\chi^{(3)}$–tensor, the $\chi^{(1)}$–tensor elements of that lattice contain nothing extraordinary and have no noticeable anisotropy.

Now let us discuss on how the above-mentioned peculiarities can be explained within a classic dipole oscillator model. We use a model approximation taking into consideration the simplest version of the anharmonicity of the oscillator potential well, which can qualitatively clarify the factors accounting for the origin of the nonlinear contribution to the polarization mechanism. The model considers an E-field induced dipole $P = Zx$ produced by the displacement x of a charge Z which is initially placed in a minimum $x = 0$ of a potential well in the monodimensional space. The curvature of the well, *i.e.* the oscillator force constant K, depends on the charge displacement x, and the model parameter $\sigma = dK(x)/dx$ characterizes such a dependence. The x value induced by the electric field E can be derived from the equilibrium between the electric and mechanical forces applied to the charge: $ZE = Kx$; $x = ZE/K$. This means that $dx/dE = Z/K$, and the expressions for the linear α and the two first nonlinear β and γ polarizabilities of the oscillator are of the following form:

- $\alpha = dP/dE = (dP/dx)\,(dx/dE) = (Z)(Z/K) = Z^2/K$ (Eq. 1)
- $\beta = d\alpha/dE = (d\alpha/dK)\,(dK/dx)\,(dx/dE) = (-Z^2/K^2)(\sigma)(Z/K) = -\sigma Z^3/K^3$ (Eq. 2)
- $\gamma = d\beta/dE = (d\beta/dK)\,(dK/dx)\,(dx/dE) = (3\sigma Z^3/K^4)(\sigma)(Z/K) = 3\sigma^2 Z^4/K^5$ (Eq. 3)

Let us remind that the α polarizability, a microscopic quantity, is the homolog of the $\chi^{(1)}$ susceptibility, a macroscopic quantity (as β for $\chi^{(2)}$ and γ for $\chi^{(3)}$).

The absence of noticeable anisotropy for the elements of the $\chi^{(1)}$–matrix (Table 4) seems to be explicable: they do not depend on the σ parameter. It readily follows from Eqs. 1-3 that the potential well anharmonicity represents the source of the dipole nonlinearity: within our model, this occurs only when the σ parameter is introduced into consideration. This fact allows us to attribute the high values of the $\chi^{(3)}_{xxxx}$ and $\chi^{(3)}_{zzzz}$ susceptibilities to the specific constitution of the molecular orbital related to the weak Te^{IV}-O bonding. Note that the occurrence of the molecular TeO^{2+} entity is indicative of the sp_y hybridization of the Te^{IV} atom. This implies that the formation of the four other bonds should result from the complementary $p_{xz}^2d^2$ hybridization and would be mainly assured by the overlap between the 'long range' d-orbitals of the Te^{IV} atom with the atomic orbitals of O atoms at 2.12 Å. Furthermore, since the spatial variability of the d-orbitals is high among those which assure the formation of covalent bonds, the σ parameter should be high when the d-orbitals play the central role in the bonding. Such a situation can be expected for the heavy element oxides, which in particular can explain why the hyperpolarizability of the long Te-O bonds should be extraordinarily high.

5. Conclusion

The results of this study improve the understanding of the specific role of the Te^{IV} atom d-orbitals in the structural and dielectric properties of crystalline complex tellurium oxides. The $BaTe_2O_6$ crystal structure presents two types of Te coordination polyhedron: one quasi-isotropic $Te^{VI}O_6$ octahedron and one highly anisotropic $Te^{IV}O_5$ tetragonal pyramid composed of one exceptionally short molecular bond (1.82 Å) oriented along the y axis and four long and weak bonds (2.12 Å), lying practically in the xz–plane. The quantitative polarizability characteristics of such bonds can thus be separately estimated from the diagonal elements of

the relevant tensors (taking into account that the contribution from the $Te^{VI}O_6$ polyhedra should be isotropic). To the best of our knowledge, such a possibility was never found for any other crystalline structure. The tensors of the linear $\chi^{(1)}$ and second-order nonlinear $\chi^{(3)}$ susceptibilities show the following features:

- No strong distinctions occur between the diagonal elements of the $\chi^{(1)}$ tensor, pointing to the fact that the magnitudes of the linear polarizabilities of both types of bond do not differ dramatically. With a simple polarizability model considering only three physical values, namely the Z, K and σ parameters, it implies that the first two of these parameters are not capable of producing strong anisotropy of the polarizability tensor.
- The xxxx– and zzzz–components of the $\chi^{(3)}$ tensor are about ten times as high as the yyyy–component, evidencing that the magnitude of the second-order nonlinear polarizability of the long bonds is much higher than that of the short one. The physical aspect of such a difference may lie in the fact that the anharmonicity of the potential wells of the Te-O dipoles related to the long bonds is much stronger than that related to the short one. We venture the opinion that the chemical aspect of such a situation is determined by the nature of the contribution from the Te^{IV} atomic orbitals to those bonds: the long bonds correspond to the p^2d^2 hybridization whereas the short bond corresponds to the sp hybridization.

Let us underline that the stability of Te-O bonds of length of about 2.1 Å is mainly assured by the d-orbitals contribution which vanishes for a length superior to 2.4 Å, causing the bonds to break [7]. Consequently, the long Te-O bonds (2.12 Å) in the $BaTe_2O_6$ lattice can be considered in a ‘precritical’ state. The very low stability of the Te^{IV} sp^3d^2 hybridization at normal conditions seems to be in the state of ‘degradation’ and begins to collapse with the occurrence of the alternative sp^3d hybridization implying a $Te^{IV}O_4$ coordination sphere of lower energy.

Besides the case of $BaTe_2O_6$, these conclusions confirm the dominating role of the axial Te-O bonds in the high $\chi^{(3)}$ hypersusceptibility of α-TeO_2, and are in line with the ideas clarifying the nature of the huge nonlinearity of the TeO_3 crystal lattice polarization [25]. Therefore, to our belief, these conclusions can have more universal validity for a wide group of heavy element oxides in which the chemical bonding is assured by the d-orbitals contribution, and in particular can clarify why the materials demonstrating extraordinary hyperpolarizability (and hypersusceptibility) have quite ordinary characteristics for the linear part of the polarization.

Acknowledgments

Calculations were performed on the CALI (Calculateur en Limousin) computer cluster of the Université de Limoges, funded by the Région Limousin, the XLIM, IPAM, GEIST institutes and the Université de Limoges. We are grateful to the Conseil Régional du Limousin for financial support.

Table captions

Table 1. Crystal data, data collection, refinement conditions and computing details for the $BaTe_2O_6$ compound.

Table 2. Atomic coordinates, displacement parameters and interatomic distances for the $BaTe_2O_6$ compound (esd are given in brackets).

Table 3. Experimental band positions (in cm^{-1}) of the Raman spectrum of the $BaTe_2O_6$ compound compared with the results of *ab initio* (with CRYSTAL06) and empirical (valence force field model with LADY) calculations.

Table 4. $\chi^{(1)}$ and $\chi^{(3)}$ susceptibilities tensors of the $BaTe_2O_6$ compound obtained by *ab initio* calculations (with SIESTA). (1 esu = 1.3982×10^{-8} $m^2.V^{-2}$)

Figure captions

Figure 1. Possible Te^{IV} environments in TeO_2–based materials according to the nature and quantity of the added modifier oxide. The Te core is in black, the O atoms in red and the Te lone electron pair is represented by a blue arrow. The longest Te-O bonds are represented by dashed lines. The given Te-O distance values are average values.

Figure 2. Displays of the $BaTe_2O_6$ structure. (a) Atomic arrangement of the unit cell. (b) Structural fragment around Te^{IV} and Te^{VI} atoms. (c) Structural fragment around a Ba atom. Te^{IV} atoms are labelled as Te1 and Te^{VI} atoms as Te2. Interatomic distances are given in Å.

Figure 3. Experimental spectra of powder-like sample of $BaTe_2O_6$ complemented by *ab initio* calculations (with CRYSTAL06) of (a) Raman scattering and (b) infrared absorption.

Figure 4. Experimental and empirically modelled (with LADY) spectra of the $BaTe_2O_6$ crystalline phase (a) with (b) without including the contribution of the Te^{IV}-$O_{(3)}$ interactions.

Figure 5. Te-O interatomic overlap population in various TeO_2– and TeO_3–based compounds calculated with CRYSTAL06 (taken from [17] and completed with the calculated values for the $BaTe_2O_6$ compound).

References

[1] S.-H. Kim, T. Yoko, S. Sakka, Linear and nonlinear optical properties of TeO_2 glass, J. Am. Ceram. Soc. 76 (1993) 2486–2490. doi:10.1111/j.1151-2916.1993.tb03970.x.

[2] M. Ben Yahia, E. Orhan, A. Beltrán, O. Masson, T. Merle-Méjean, A. Mirgorodski, et al., Theoretical third-order hyperpolarizability of paratellurite from the finite field perturbation method, J. Phys. Chem. B. 112 (2008) 10777–10781. doi:10.1021/jp805050s.

[3] N. Berkaïne, E. Orhan, O. Masson, P. Thomas, J. Junquera, Nonlinear optical properties of TeO_2 crystalline phases from first principles, Phys. Rev. B. 83 (2011) 245205. doi:10.1103/PhysRevB.83.245205.

[4] S. Suehara, P. Thomas, A.P. Mirgorodsky, T. Merle-Méjean, J.C. Champarnaud-Mesjard, T. Aizawa, et al., Localized hyperpolarizability approach to the origin of nonlinear optical properties in TeO_2-based materials, Phys. Rev. B. 70 (2004) 205121.

[5] A.P. Mirgorodsky, M. Soulis, P. Thomas, T. Merle-Méjean, M. Smirnov, Ab initio study of the nonlinear optical susceptibility of TeO_2-based glasses, Phys. Rev. B. 73 (2006) 134206. doi:10.1103/PhysRevB.73.134206.

[6] M. Soulis, T. Merle-Méjean, A.P. Mirgorodsky, O. Masson, E. Orhan, P. Thomas, et al., Local molecular orbitals and hyper-susceptibility of TeO_2 glass, J. Non-Cryst. Solids. 354 (2008) 199–202. doi:10.1016/j.jnoncrysol.2007.07.036.

[7] M. Smirnov, A. Mirgorodsky, O. Masson, P. Thomas, Quantum mechanical study of pre-dissociation enhancement of linear and nonlinear polarizabilities of $(TeO_2)_n$ oligomers as a key to understanding the remarkable dielectric properties of TeO_2 glasses, J. Phys. Chem. A. 116 (2012) 9361–9369. doi:10.1021/jp303014k.

[8] P.A. Thomas, The crystal structure and absolute optical chirality of paratellurite, α-TeO_2, J. Phys. C Solid State Phys. 21 (1988) 4611–4627.

[9] H. Beyer, Refinement of the crystal structure of tellurite, the orthorhombic TeO_2, Z. Für Krist. Krist. Krist. Krist. 124 (1967) 228–237.

[10] J.C. Champarnaud-Mesjard, S. Blanchandin, P. Thomas, A. Mirgorodsky, T. Merle-Méjean, B. Frit, Crystal structure, Raman spectrum and lattice dynamics of a new metastable form of tellurium dioxide: γ-TeO_2, J. Phys. Chem. Solids. 61 (2000) 1499–1507. doi:10.1016/S0022-3697(00)00012-3.

[11] S. Neov, V. Kozhukharov, I. Gerasimova, K. Krezhov, B. Sidzhimov, A model for structural recombination in tellurite glasses, J. Phys. C Solid State Phys. (1979) 2475.

[12] T. Sekiya, N. Mochida, A. Ohtsuka, M. Tonokawa, Raman spectra of $MO_{1/2}$-TeO_2 (M = Li, Na, K, Rb, Cs and Tl) glasses, J. Non-Cryst. Solids. 144 (1992) 128–144. doi:10.1016/S0022-3093(05)80393-X.

[13] Y. Himei, A. Osaka, T. Nanba, Y. Miura, Coordination change of Te atoms in binary tellurite glasses, J. Non-Cryst. Solids. 177 (1994) 164–169. doi:10.1016/0022-3093(94)90526-6.

[14] C.R. Becker, S.L. Tagg, J.C. Huffman, J.W. Zwanziger, Crystal structures of potassium tetratellurite, $K_2Te_4O_9$, and potassium ditellurite, $K_2Te_2O_5$, and structural trends in solid alkali tellurites, Inorg. Chem. 36 (1997) 5559–5564.

[15] J.C. McLaughlin, J.W. Zwanziger, Modeling glasses using the reverse Monte Carlo algorithm: addition of nuclear magnetic resonance and expanded coordination number

constraints, J. Mol. Graph. Model. 17 (1999) 275–284. doi:10.1016/S1093-3263(99)00035-2.
[16] B.O. Loopstra, K. Goubitz, The structures of four caesium tellurates, Acta Crystallogr. C42 (1986) 520–523.
[17] D. Hamani, A. Mirgorodsky, O. Masson, T. Merle-Méjean, M. Colas, M. Smirnov, et al., Crystal chemistry peculiarities of $Cs_2Te_4O_{12}$, J. Solid State Chem. 184 (2011) 637–643. doi:10.1016/j.jssc.2011.01.027.
[18] M. Koçak, C. Platte, M. Trömel, Barium hexaoxoditellurate(IV,VI): oxygen coordination number 5 at tetravalent tellurium, Acta Crystallogr. B35 (1979) 1439–1441.
[19] R. Dovesi, R. Orlando, B. Civalleri, C. Roetti, V.R. Saunders, C.M. Zicovich-Wilson, CRYSTAL: a computational tool for the *ab initio* study of the electronic properties of crystals, Z. Für Krist. 220 (2005) 571–573. doi:10.1524/zkri.220.5.571.65065.
[20] R. Dovesi, V.R. Saunders, C. Roetti, R. Orlando, C.M. Zicovich-Wilson, F. Pascale, et al., CRYSTAL06 User's Manual, University of Torino, Torino, Italy, 2006. www.crystal.unito.it/Manuals/crystal06.pdf.
[21] A.D. Becke, Density-functional thermochemistry. III. The role of exact exchange, J. Chem. Phys. 98 (1993) 5648–5652.
[22] C. Lee, W. Yang, R.G. Parr, Development of the Colle-Salvetti correlation-energy formula into a functional of the electron density, Phys. Rev. B. 37 (1988) 785–789.
[23] M.B. Smirnov, V.Y. Kazimirov, LADY: software for lattice dynamics simulations, JINR Commun. E14 (2001) 159.
[24] A.P. Mirgorodsky, T. Merle-Méjean, J.-C. Champarnaud, P. Thomas, B. Frit, Dynamics and structure of TeO_2 polymorphs: model treatment of paratellurite and tellurite; Raman scattering evidence for new γ- and δ-phases, J. Phys. Chem. Solids. 61 (2000) 501–509. doi:10.1016/S0022-3697(99)00263-2.
[25] A. Plat, J. Cornette, M. Colas, A.P. Mirgorodsky, M.B. Smirnov, O. Noguera, et al., Huge susceptibility increase within the $(1-x)\ TeO_2 + x\ TeO_3$ crystal system: Ab initio calculation study, J. Alloys Compd. 587 (2014) 120–125. doi:10.1016/j.jallcom.2013.10.126.
[26] J.M. Soler, E. Artacho, J.D. Gale, A. García, J. Junquera, P. Ordejón, et al., The SIESTA method for ab initio order-N materials simulation, J. Phys. Condens. Matter. 14 (2002) 2745. doi:10.1088/0953-8984/14/11/302.
[27] J.P. Perdew, K. Burke, M. Ernzerhof, Generalized gradient approximation made simple, Phys. Rev. Lett. 77 (1996) 3865–3868. doi:10.1103/PhysRevLett.77.3865.
[28] J.P. Perdew, K. Burke, M. Ernzerhof, Errata: Generalized gradient approximation made simple, Phys. Rev. Lett. 78 (1997) 1396–1396. doi:10.1103/PhysRevLett.78.1396.
[29] N. Troullier, J.L. Martins, Efficient pseudopotentials for plane-wave calculations, Phys. Rev. B. 43 (1991) 1993–2006. doi:10.1103/PhysRevB.43.1993.
[30] L. Kleinman, D.M. Bylander, Efficacious form for model pseudopotentials, Phys. Rev. Lett. 48 (1982) 1425–1428. doi:10.1103/PhysRevLett.48.1425.
[31] S. Adams, Relationship between bond valence and bond softness of alkali halides and chalcogenides, Acta Crystallogr. B57 (2001) 278–287.
[32] S. Adams, soft BV (version 0.96), (2004). http://www.softBV.net.
[33] M. Soulis, A.P. Mirgorodsky, T. Merle-Méjean, O. Masson, P. Thomas, M. Udovic, The role of modifier's cation valence in structural properties of TeO_2-based glasses, J. Non-Cryst. Solids. 354 (2008) 143–149. doi:10.1016/j.jnoncrysol.2007.07.032.
[34] K.C. Krasnov, H.B. Filippenko, B.A. Bobkov, Молекулярные постоянные неорганических соединений (Molecular constants of inorganic compounds), Л.: Химия, 1979.

[35] D. Yakovlev, A. Mirgorodskii, A. Tulub, B. Shchegolev, Nonempirical calculation of linear and nonlinear polarizability of TeO_2-based molecular clusters and piezoelectric properties of crystalline tellurium oxide, Opt. Spectrosc. 92 (2002) 449–454. doi:10.1134/1.1465473.

Table_1 (revised)

Crystal data	
$BaTe_2O_6$	M = 488.54
orthorhombic, n° 63, Cmcm, D_{2h}^{17}	$\rho = 6.242$ g.cm^{-3}
Z = 4	$\mu = 18.592$ mm^{-1}
a = 5.562(2) Å	T = 293(2) K
b = 12.773(5) Å	Mo Kα radiation
c = 7.318(3) Å	prismatic, colourless
V = 519.9(3) Å^3	0.02 × 0.01 × 0.01 mm
Data collection	
Bruker-Nonius KappaCCD area-detector diffractometer	$T_{min} = 0.765$, $T_{max} = 0.830$
measured reflections = 8832	$h = -9 \rightarrow 9$
independent reflections = 804	$k = -22 \rightarrow 22$
reflections with $I > 2\sigma(I)$ = 689	$l = -12 \rightarrow 12$
$R_{int} = 0.0398$	$\theta_{min} = 4.872°$, $\theta_{max} = 39.287°$
Refinement	
R = 0.0160	804 reflections
wR = 0.0303	31 parameters
GooF = 1.066	$\Delta\rho_{min} = -1.592$ e.Å^{-3}, $\Delta\rho_{max} = 1.382$ e.Å^{-3}
Computing details	
Data collection: COLLECT [19]; absorption correction: SADABS [20]; cell refinement: DirAx/LSQ [21]; data reduction: EVALCCD [22]; program used to solve structure: SHELXS97 [23]; program used to refine structure: SHELXL-2014/7 [23]; molecular graphics: Diamond [24]; software used to prepare material for publication: publCIF [25].	

Table_2 (revised)

Atomic coordinates and isotropic or equivalent isotropic displacement parameters (in $Å^2$)								
Atom	Ox.	Wyck.	Sym.	x	y	z	U_{eq}	Site occupancy
Ba	+2	4c	m2m	0.	0.71847(2)	0.75	0.01217(6)	1.
Te^{IV}	+4	4c	m2m	0.5	0.91413(2)	0.75	0.00482(6)	1.
Te^{VI}	+6	4a	2/m..	0.	0.	0.5	0.00361(6)	1.
$O_{(1)}$	-2	4c	m2m	0.	0.0465(2)	0.75	0.0112(6)	1.
$O_{(2)}$	-2	4c	m2m	0.5	0.7714(2)	0.75	0.0087(5)	1.
$O_{(3)}$	-2	16h	1	0.7635(3)	0.89498(10)	0.54382(19)	0.0093(2)	1.

Interatomic distances (Å)						
Te^{IV}-$O_{(2)}$	1.823(3)	x 1	Ba-$O_{(2)}$	2.8621(12)	x 2	
Te^{IV}-$O_{(3)}$	2.1176(15)	x 4	Ba-$O_{(3)}$	2.9785(16)	x 4	
Te^{VI}-$O_{(3)}$	1.9059(14)	x 4	Ba-$O_{(3)}$	3.0149(17)	x 4	
Te^{VI}-$O_{(1)}$	1.9234(11)	x 2				

Table_3

experimental	*ab initio*	VFF	VFF (without Te^{IV}-$O_{(3)}$ contribution)
59	69 A_g	58 A_g	57 A_g
155	159 A_g	99 A_g	96 A_g
289	286 A_g	254 A_g	193 A_g
424	425 A_g	437 A_g	429 A_g
513	527 A_g	514 A_g	500 A_g
708	714 A_g	717 A_g	712 A_g
790	819 A_g	788 A_g	776 A_g

Table_4

$\chi^{(1)}$ tensor elements	no unit	$\chi^{(3)}$ tensor elements	$\times 10^{-13}$ esu
xx	4.2	xxxx	30.0
yy	2.3	yyyy	3.2
zz	3.4	zzzz	44.3

Figure_1

‘Classical’ environments

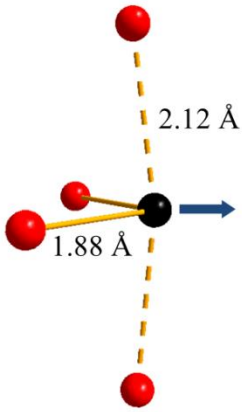

TeO_4

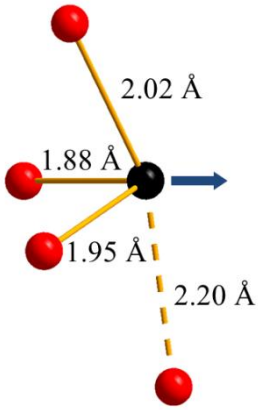

TeO_{3+1}

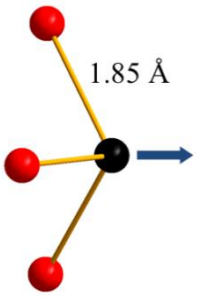

TeO_3

‘Unclassical’ environments

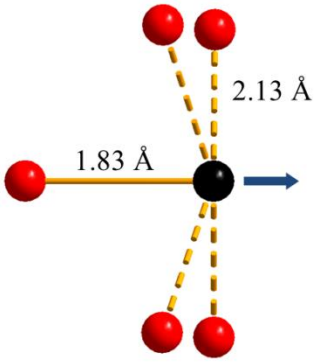

TeO_5 (in $BaTe_2O_6$ [18])

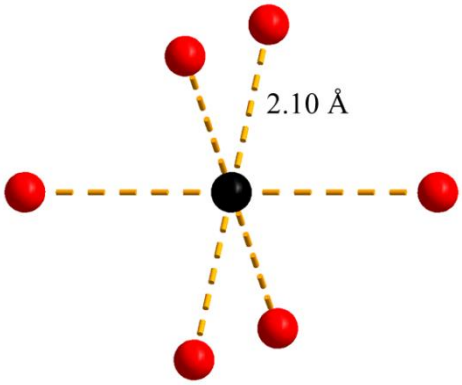

TeO_6 (in $Cs_2Te_4O_{12}$ [16])

Figure_2

(a)

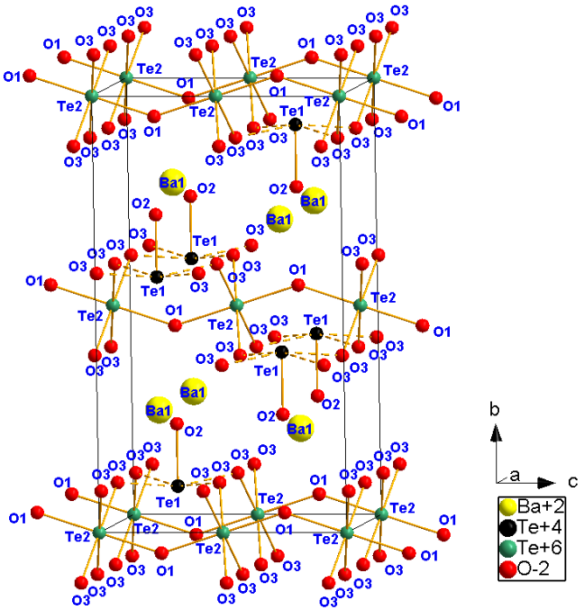
Ba1
Te1
Te2
O1
O2
O3
b
a
c
Ba+2
Te+4
Te+6
O-2

(b)

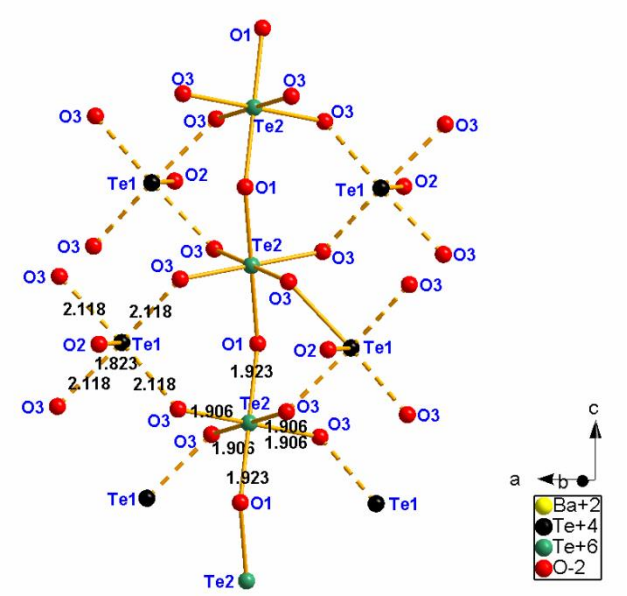
O1
O2
O3
Te1
Te2
2.118
1.823
1.923
1.906
c
a
b
Ba+2
Te+4
Te+6
O-2

(c)

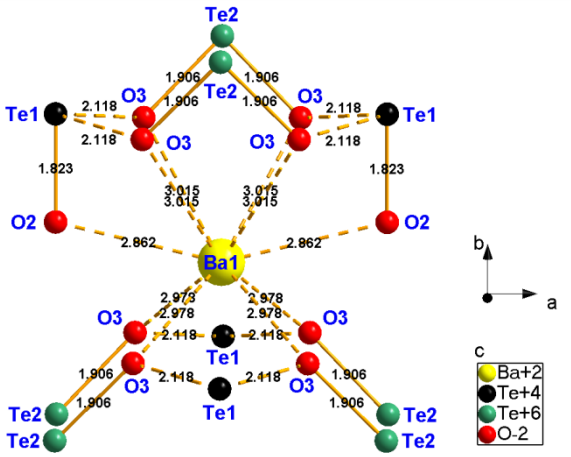
Te1
Te2
O2
O3
Ba1
1.823
2.118
1.906
2.862
2.973
2.978
3.015
b
a
c
Ba+2
Te+4
Te+6
O-2

Figure_3

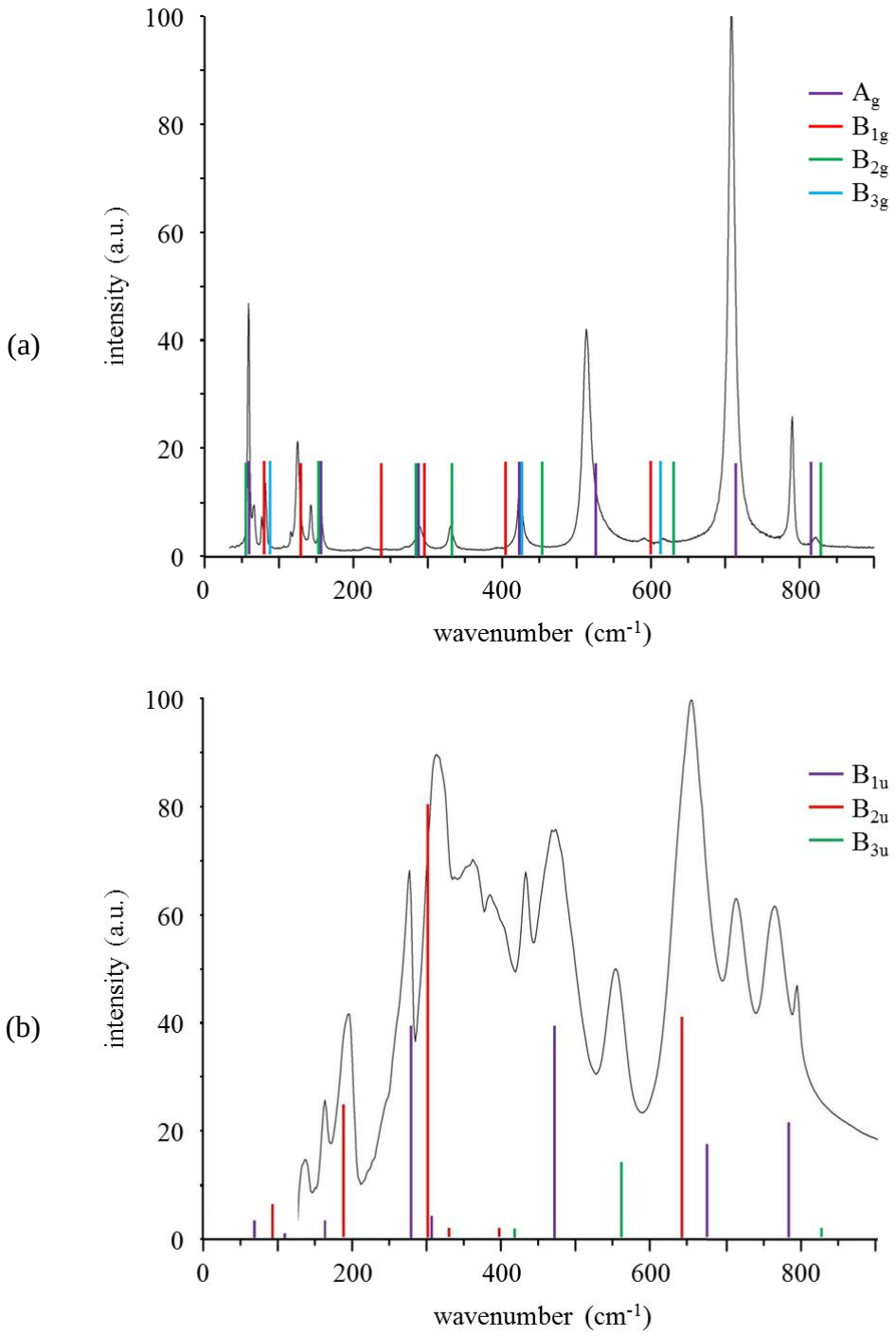
(a)
intensity (a.u.)
wavenumber (cm-1)
Ag
B1g
B2g
B3g
(b)
intensity (a.u.)
wavenumber (cm-1)
B1u
B2u
B3u

Figure_4

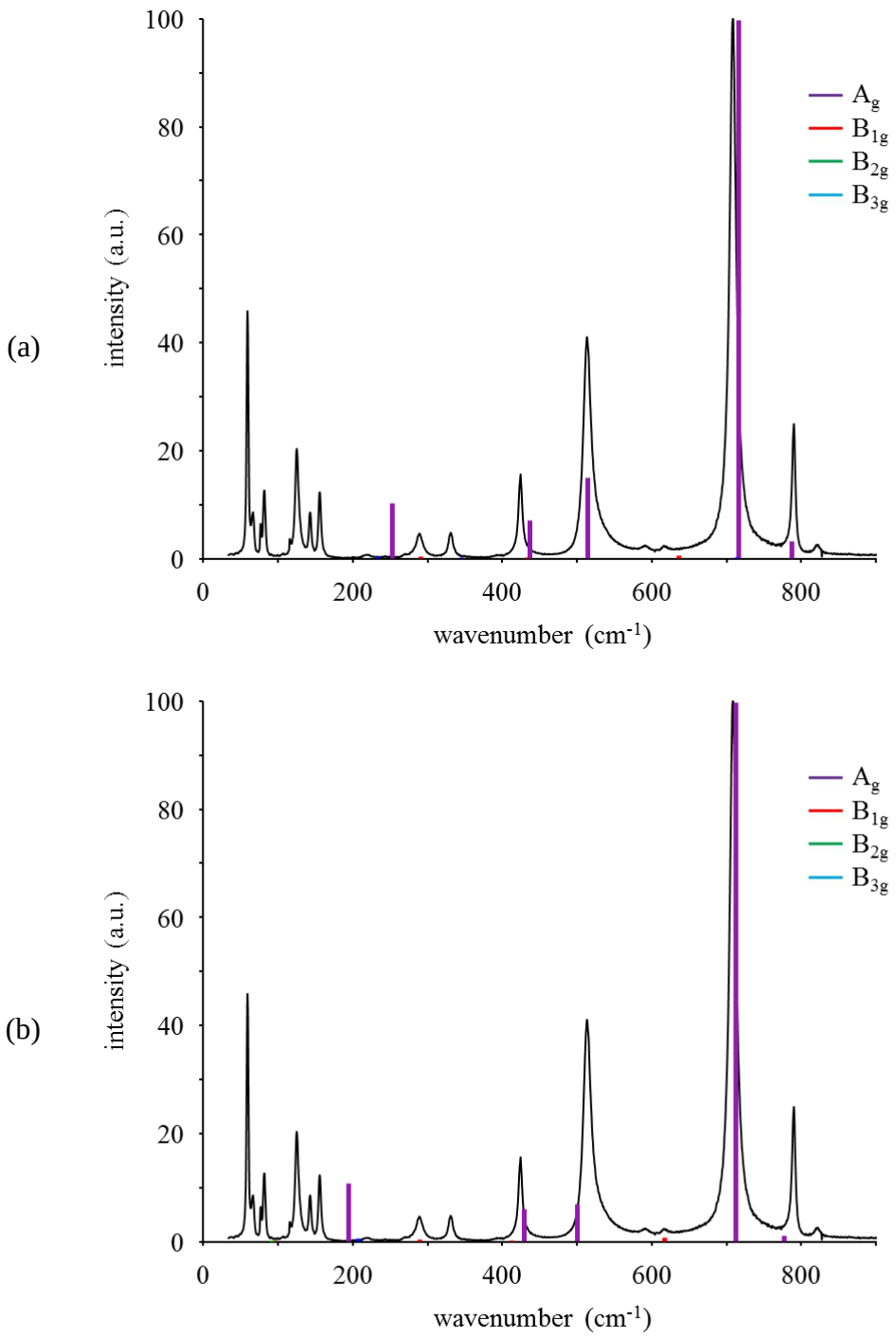
(a)
intensity (a.u.)
wavenumber (cm-1)
Ag
B1g
B2g
B3g
(b)
intensity (a.u.)
wavenumber (cm-1)
Ag
B1g
B2g
B3g

Figure_5

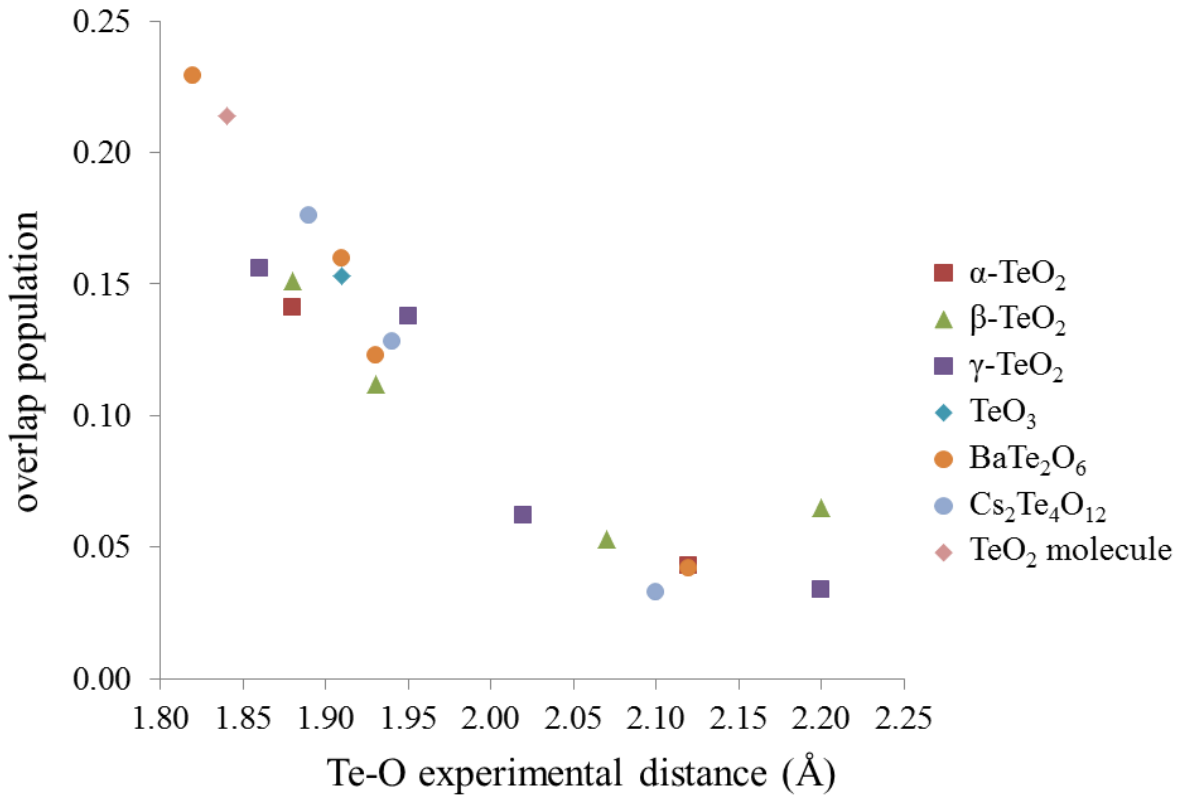
0.25
0.20
0.15
0.10
0.05
0.00
overlap population
1.80
1.85
1.90
1.95
2.00
2.05
2.10
2.15
2.20
2.25
Te-O experimental distance (Å)
α-TeO2
β-TeO2
γ-TeO2
TeO3
BaTe2O6
Cs2Te4O12
TeO2 molecule